

Multi-material Fabrication for Magnetically Driven Miniature Soft Robots Using Stereolithography

Zhaoxin Li and Eric Diller

Abstract—Remote manipulation and controlled navigation of magnetically driven miniature soft robots make them promising robotic tools operating in hard-to-reach workspace. The functionality of robots can be enhanced by integrating multiple materials with different mechanical or magnetic characteristics. However, it remains challenging combining multiple materials along with arbitrary magnetization profile formation during fabrication. This study, from a pixel level, uses stereolithography process to precisely incorporate multiple materials with different physical properties for millimeter-scale robot printing, as well as encode discrete magnetizations for the actuating parts, which provides a customizable approach for sophisticated shape production. Complex shape transformations and dynamic motions were observed through the magnetic actuation of printed robots. With the integration of magnetoactive and non-magnetic materials, free locomotion in a liquid environment tracked by optical and ultrasonic detections was achieved by actuating a 4-arm flapping robot. Moreover, discrete patterns were formed with the combination of soft and rigid magnetic materials. Such versatility of robotic behaviors and enhanced morphing capabilities enable the creation of complex multi-material actuators and provide a promising route towards a wide spectrum of biomedical applications.

Keywords: soft robots, multi-material printing, magnetic actuation, digital light processing

I. INTRODUCTION

Reversible shape transformations created by actuation systems with high design complexity are pervasive in natural organisms. By programming soft robots with smart materials, the printed structures show the capabilities of implementing complex transformations such as gripping [1]–[3], crawling [4]–[6], swimming [7]–[10] or multimodal behaviours [11]–[14] in response to thermal [2], [15], electric [3], [16], light [5], [17] or magnetic [1], [4], [6]–[14] stimuli. Among these responsive mechanisms, magnetic actuation shows great advantages in untethered manipulation due to the fast response of magnetic structures to the applied magnetic field. Magnetoactive materials that consist of embedded magnetic particles and soft polymer matrices are ideal candidates for the magnetically driven soft robot fabrication. On-demand dynamic motions and shape reconfigurations of robots can be achieved through the process of magnetic field maneuvers, which can be potentially applied for drug delivery, object manipulation, or micro assembly.

However, single-material actuators have limited capabilities operating in sophisticated task environments where multiple objectives or functions are required. On

the one hand, integration of multiple materials provides possibilities to incorporate multiple types of stimuli on one actuator. Previous work has combined magnetic actuation with thermal [11] and light [18] stimuli. On the other hand, multi-material mechanisms bond materials with varying physicochemical characteristics that can be exploited independently to enhance the complexity and dexterity of the actuator. The combination of soft and rigid materials facilitates large deformations or complex motions for the designed structure [19], while integrating magnetoactive and non-magnetic segments materials elevates the morphing capability or manipulation efficiency of the robots [13], [20]–[22]. Moreover, enhanced functionalities and magnetic responsiveness are observed by integrating dissimilar materials with distinct properties that can be engineered in parallel [23].

Different fabrication methods have been used for the multi-material fabrication, which involve two photon polymerization [19], [23], [24], direct ink writing [11], drop-on-demand 3D printing [25] and digital light processing (DLP) [21], [26]. However, incorporating multiple materials with high manufacturing precision on the micro scale remains challenging. Methods involving mold processing or manual assembly restrict the shape complexity of fabricated samples and increase the time cost. Studies incorporating multiple materials using DLP [21], [26] approximate each actuating part as a point dipole and use concentrated fields generated by the permanent magnet to actuate the magnetoactive segment. Such actuation scheme relies on the maneuver of permanent magnet in close proximity, thus making the remote manipulation difficult under complex circumstances. In this work, we use digital process to precisely bond multiple materials. Meanwhile, the magnetoactive segments are encoded with arbitrary magnetization profiles as our previous work has demonstrated [27]. The printed structures undergo complex shape transformations under the uniform field and show high flexibility and durability at the interface of different materials. The introduction of multiple materials enhances the dynamic performance and the morphing capability of small robots. In addition, the customized shape designs can be produced within minutes, which enables 3D production of miniature robots with a high degree of automation and reproducibility.

In this work, two types of photopolymer: a rigid type and a soft type were introduced as the polymer matrix, and NdFeB nanoparticles were embedded to generate the magnetism. With the integration of magnetoactive and non-magnetic

Z. Li and E. Diller are with the department of Mechanical and Industrial Engineering, University of Toronto, 5 King's College Road, Toronto M5S 3G8, Canada (email: lzx.lee@mail.utoronto.ca, ediller@mie.utoronto.ca)

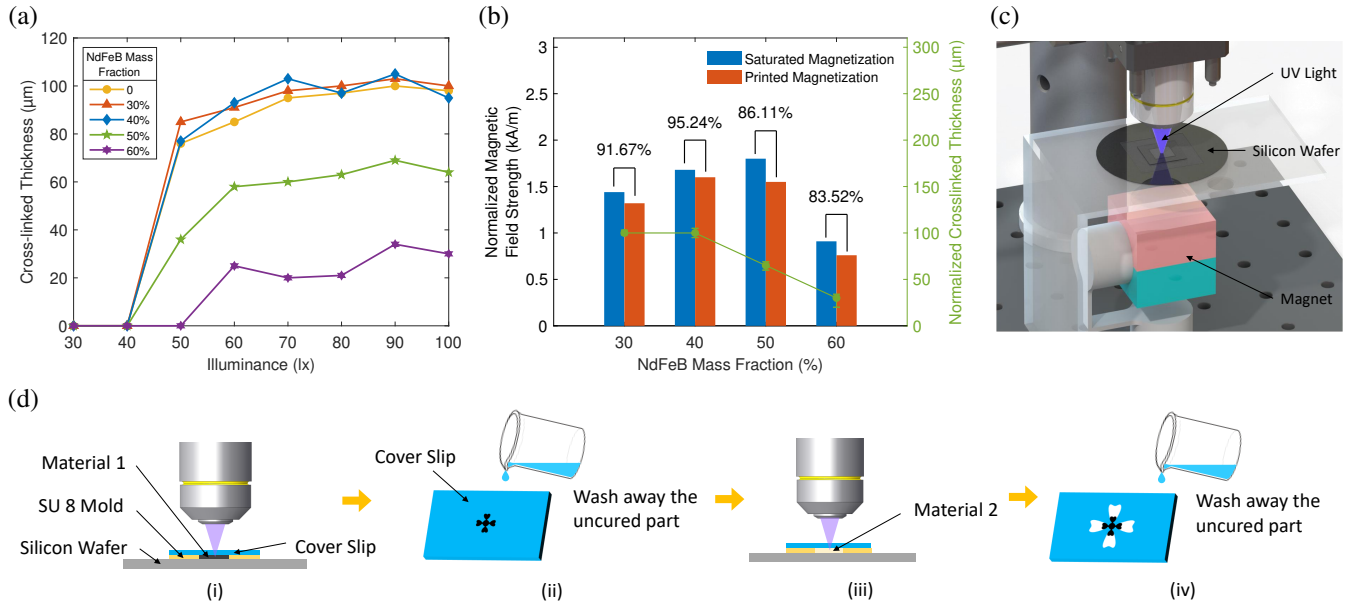


Fig. 1: Magnetic composite and fabrication process. (a) Crosslinked thickness of samples with varying NdFeB mass fractions under different illuminance. (b) Normalized magnetic field strength at the near surface of printed samples with printed magnetization and saturated magnetization. The percentage indicates the ratio of printed magnetization to saturated magnetization in terms of magnetic field strength. The normalized crosslinked thickness corresponds to the median value of saturated crosslinked thickness in repeated tests. (c) Physical apparatus to fabricate customized shapes with discrete magnetization profiles. The UV light pattern is generated by a DLP projector and focused on the silicon wafer through a group of lens. A cubic magnet is placed below to generate the alignment field for magnetic nanoparticles' reorientation. (d) Process of multi-material fabrication. (i) Material 1 is filled in the mold and gets cured. (ii) The cured part of material 1 sticks to the cover slip, and the uncured part is washed by the deionized (DI) water and gets removed. (iii) The cover slip containing the cured part of material 1 is placed back and aligned. Material 2 is filled in the mold and gets cured. (iv) The uncured part of material 2 is washed and removed.

soft materials, non-reciprocal motions were observed when actuating a 4-arm flapping robot. Meanwhile, a beam shape with multiple segments was produced by combining soft and rigid materials, which then formed a discrete deflection pattern under field actuation.

II. MATERIALS AND METHODS

A. Magnetic Composite

The magnetic material is composed of NdFeB nanoparticles and photopolymer. The transparency of material varies for different NdFeB mass fractions, which affects the crosslinked thickness of structural layer when getting exposed to the ultraviolet (UV) light during fabrication process. The magnetic composite is filled into a gap formed by glass cover slip, SU-8 mold and silicon wafer. The SU-8 mold is prepared using photolithography, and the gap width is $\sim 100 \mu\text{m}$. Fig. 1 (a) shows the layer thickness with varying NdFeB mass fractions under different illuminance. The crosslinked thickness becomes stable when the illuminance is beyond 70 lx. For samples with NdFeB mass fractions of 0, 30% and 40%, the crosslinked thickness gets saturated and equals the gap width of $\sim 100 \mu\text{m}$. As we further increase the NdFeB mass fraction, the saturated crosslinked thickness becomes smaller, which is $\sim 65 \mu\text{m}$ and $\sim 30 \mu\text{m}$ for NdFeB mass fractions of 50% and 60%, respectively. Samples are not cured or fully cured under low illuminance, which corresponds to the thickness of zero.

The magnetization of printed samples with varying NdFeB mass fractions was evaluated by measuring the

magnetic field strength at the near surface of printed samples. In our test, squared samples with the size of $3.7 \text{ mm} \times 3.7 \text{ mm}$ and 90° out-of-plane magnetization were placed onto a planar magneto-optical sensor (MagView S, Matesy GmbH, Germany). The out-of-plane magnetic field strength was measured for samples with printed magnetization and saturated magnetization. The printed magnetization is the reorientation result of embedded pre-magnetized nanoparticles under alignment field, and the saturated magnetization is obtained by placing the same printed sample into a large uniform magnetic field to get fully magnetized.

The normalized magnetic field strength was computed as the average magnetic field strength within the span of the structure at the near surface of printed sample. Fig. 1 (b) compares the normalized magnetic field strength for samples with printed magnetization and saturated magnetization. The crosslinked thickness decreases as the NdFeB mass fraction becomes larger, meaning the volume of the sample structure becomes smaller, which contributes to the decline of normalized magnetic field strength. In addition, the magnetic slurry becomes viscous as we increase the NdFeB mass fraction, which makes it hard for embedded NdFeB particles to reorient with the alignment field, thus resulting in a decreased percentage of printed magnetization to saturated magnetization. The optimal NdFeB mass fraction that we use for the following experiments is chosen as 40%, since it has the largest normalized magnetic field strength with

printed magnetization and the maximum percentage of printed magnetization to saturated magnetization.

B. Fabrication Method

Various types of magnetic materials were prepared by mixing NdFeB nanoparticles with different polymer matrices. The permanent magnetic particles (D50 = 5 μm , MQFP-15-7, NdPrFeB, Magnequench (Tianjin) Co. Ltd., Tianjin, China) were firstly magnetized in a strong uniform magnetic field (2.3 T) generated by an impulse magnetizer (9 Tesla Pulse Magnetiser, Magnetic Measurements Ltd., Lancashire, UK) to get the saturation remanence. They were then mixed with soft UV resin (Elastic 50A, Formlabs Inc., MA, USA) or rigid UV resin (Clear V4, Formlabs Inc., MA, USA) and stirred by a glass rod for 5 minutes to form a homogeneous magnetic slurry. After removing bubbles in a vacuum degassing chamber for 1 minute, the magnetic slurry was transferred into a 8 mm \times 8 mm \times 0.1 mm SU-8 mold. The magnetic composite was then placed under a DLP projector (DLP LightCrafter 4500, modified with a 405-nm light engine, Texas Instruments Inc., TX, USA). The embedded magnetic particles were reoriented by the alignment field generated by a cubic permanent magnet below the working platform and held for 2 minutes (shown as Fig. 1 (c)). After that, the region of interest was exposed to the blue light (405 nm, 80 lx) for 2.5 seconds to fix the magnetization direction. The reorienting and curing steps were alternated for a few more cycles to get the customized magnetization profile.

Fig. 1 (d) shows the process of multi-material fabrication. The first material was prepared and filled into the mold to get cured with customized shapes. Since the cured segment was exposed to the UV light, the contour of illuminated area was captured by a CMOS camera mounted on top and drawn on the screen. After the first material was printed, the cured part adhered to the cover slip while the uncured part was washed and removed by deionized water. Then the second material was transferred into the mold and the cover slip containing first material was placed back onto the working platform. The printed structure of first material was aligned with the contour drawn previously, then the UV light pattern was projected to get the second material cured. The curing and washing steps were repeated when more materials were included, and the process of magnetic alignment was added before the curing step to encode the magnetization profile in presence of magnetoactive materials. At the end of the process, the printed structure was washed and peeled off from the cover slip to get our final product.

III. EXPERIMENTS AND RESULTS

A. Integration of magnetoactive and non-magnetic materials

Compared with structures solely made of magnetoactive materials, incorporation of magnetoactive and non-magnetic segments could enhance robot's dynamic performance under magnetic actuation. When actuated by an external magnetic field, the embedded magnetic particles in the polymer matrix can generate microtorques to align the

magnetoactive segment with the direction of external field. The non-magnetic segments generate no response to the magnetic actuation, which can be attached as flexible joints or passive parts of motions.

1) *4-arm flapping robot*: As promising miniaturized robotic tools that can operate in small enclosed spaces, untethered swimming robots with small size have great potentials being applied for targeted drug delivery, tissue sampling or minimal invasive surgery. Previous studies have designed different types of swimming structures including flapping-wing robots [28], jellyfish-like robots [10], helical microswimmers [8], [29] and ciliary robots [9] to mimic the swimming of natural organisms. Some of these studies utilize non-reciprocal motion as the swimming mechanism to generate propelling force for the robot. Integration of magnetoactive and non-magnetic materials can provide a good solution for the formation of non-reciprocal motion.

In this work, a flapping robot with 4 arms was fabricated by integrating magnetoactive and non-magnetic materials. The magnetoactive material was prepared by mixing NdFeB nanoparticles with soft UV resin. Fig. 2 (a) shows the magnetization profile of the robot. The arms of the robot bend downwards when the magnetic field is applied towards +z axis and get recovered to the initial positions when the field is removed. Flapping motions can be generated by applying an oscillating field, and the non-magnetic segments move passively as the magnetoactive segment flaps. When deployed into a fluid environment, the whole arm undergoes a non-reciprocal motion in an oscillating cycle, resulting in a net thrust force. The printed robot is illustrated as Fig. 2 (b), of which the size is \sim 5 mm from tip to tip.

2) *Magnetization strengthening*: As previously reported, the printed magnetization is the reorientation result of pre-magnetized nanoparticles, of which the intensity of magnetization is weaker than that of the saturated magnetization. This is due to the partial alignments of magnetic dipoles in the polymer matrix under weak reorientation field. To obtain a greater amplitude of deformation under a relatively small actuation field, a larger magnetization is required. In our case, the actuation field generated by electromagnetic coils can only reach a maximum magnitude of 20 mT. Therefore, the magnetization strengthening process is introduced to increase the intensity of magnetization for the flapping robot.

The key of the process is to maintain the structure's original magnetization profile. For the structure with complicated deformed shapes, it is laborious to manually hold or use molding to fix the deformation for each part of the structure before getting exposed to the magnetization field. Thus, a neat and precise way is required. Since the magnetic anisotropy has been created by the magnetization profile encoding, the structure will get fully deformed under an intermediate magnetic field. Therefore, we propose to hold the deformed shape by a small magnet and then apply a large field generated by the impulse magnetizer to saturate the magnetization of the structure. The direction of the impulse field is the same as the magnetic moment

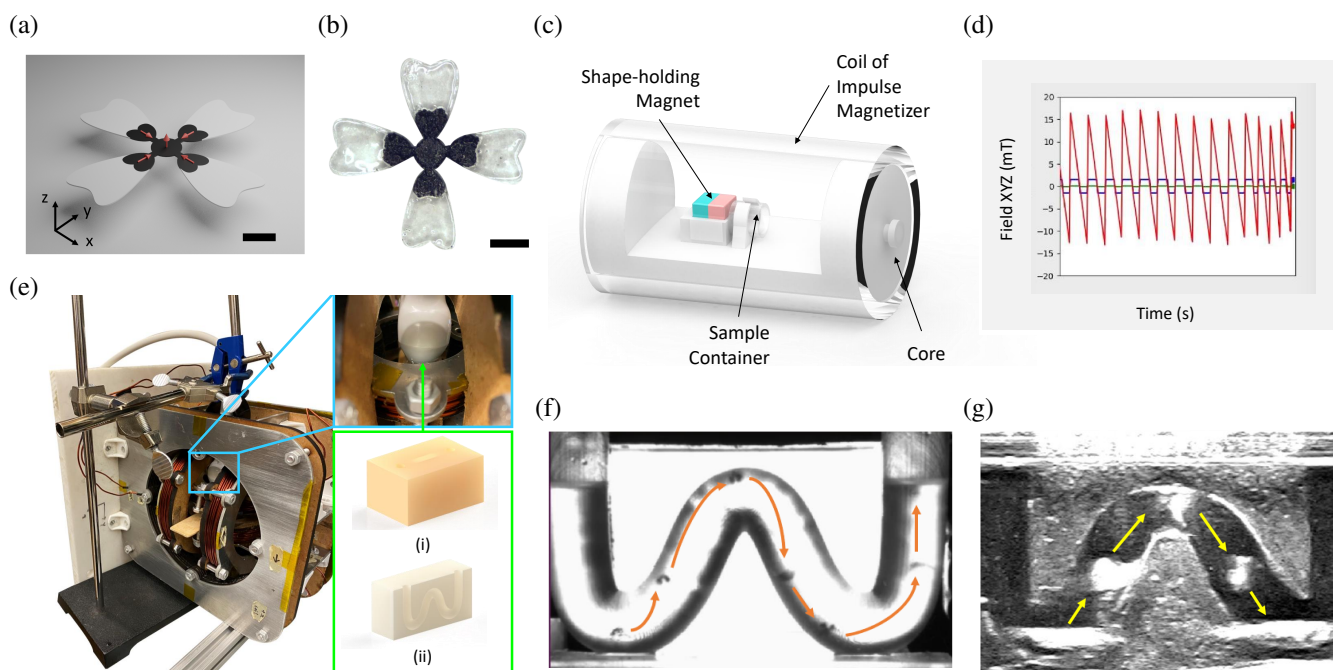


Fig. 2: Fabrication and actuation for robots with magnetoactive and non-magnetic materials. (a) Schematic representation of a 4-arm flapping robot that has the magnetization profile indicated by red arrows. The black part represents the magnetoactive segment and the grey parts correspond to non-magnetic segments. (b) Image of the printed flapping robot. The size of the robot from tip to tip is ~ 5 mm. (c) Schematic of the magnetization strengthening setup. (d) Signal pattern of the applied magnetic field for robot actuation. Fields along x, y and z directions are indicated by blue, green and red, respectively. (e) Physical setup for the ultrasonic detection of robot's motion in a curved hollow channel. The agar gel block is placed at the center of the 3-axis electromagnetic coil system. The ultrasonic probe is mounted on top and the transducer gets in contact with the agar gel block from the top surface. (i) Isometric view of the agar gel block. (ii) Cross section of the hollow structure. (f) Robot's navigation in a 3D printed curved channel under optical tracking. Orange arrows show the locomotion trajectory. (g) Robot's navigation in the hollow channel under ultrasonic detection. Yellow arrows indicate the locomotion trajectory. Scale bar, 1 mm.

direction of the small magnet. Fig. 2 (c) shows the setup used for the magnetization strengthening. First we place the printed structure into the sample container, then we clamp the container next to the shape-holding magnet mounted on the core to get the structure deformed, finally we insert the core into the coil of the impulse magnetizer and apply a large impulse field (2.3 T) to finish the magnetization strengthening.

3) *Robot Navigation*: The flapping robot was deployed into the actuation field to navigate in a liquid environment after being treated with the magnetization strengthening. A sawtooth field along the vertical axis is applied to levitate the robot while small field components along horizontal directions are superposed for the steering. However, since the net magnetic moment of the robot points at +z axis, the heading direction of the robot keeps switching up and down when we oscillate the field, thus disabling it to levitate. Such heading reversal can be prevented by modulating the actuation field or increasing the liquid viscosity. Several types of actuation field including sinusoidal, triangular and sawtooth waves were investigated. Among these, the sawtooth wave was demonstrated as the most efficient actuation signal for the robot's levitation. As Fig. 2 (d) shows, the sharp rise of the field signal contracts the robot's arms with a large beating amplitude while the ramp phase makes the arms recovered. It is noted that to eliminate the

heading reversal, the magnitude of negative part needs to be smaller than that of positive part and a relatively high frequency is required. Thus, we keep the frequency range of the oscillating field from 3.5 Hz to 7.5 Hz.

Two types of detection methods optical and ultrasonic detections, were used to track the motion of the flapping robot. In optical tracking, a clear 3D curved channel was fabricated using a commercial 3D printer. The robot was deployed into the channel filled with 60% v/v glycerol. Then the whole setup was placed into an electromagnetic coil system with three pairs of coils nested orthogonally that generates uniform magnetic fields in 3D space. The actuation field was modulated by a joystick and the robot's motion was captured by a CMOS camera (FO134TC, FOculus, Germany) from the side of the coil system. As Fig. 2 (f) illustrates, the robot successfully locomotes from the left bottom of the channel to the air-liquid interface on the right. Meanwhile, to demonstrate the enhanced locomotion capability of incorporating non-magnetic segment, the flapping robot with magnetoactive segment only was fabricated for comparison. It turned out the single-material structure failed to levitate in the same actuation scenario.

However, for most in-vivo experiments, the internal environments of biological tissues are hidden. Therefore, the ultrasound imaging is introduced to track robot's location in such application scenarios. A hollow channel in the agar gel

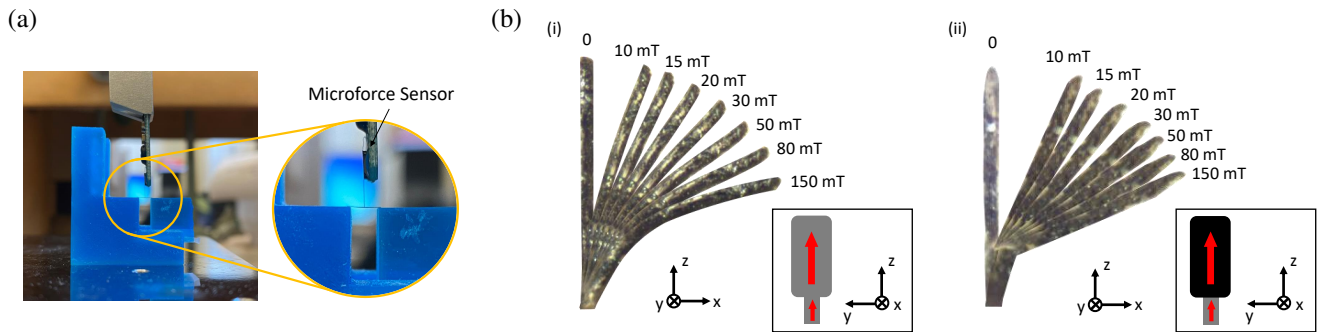


Fig. 3: Deflection characterization and beam design with the integration of soft and rigid materials. (a) Setup for three-point flexural test. (b) Deflection pattern of (i) single-material beam and (ii) multi-material beam. The soft and rigid materials are shown as grey and black, respectively. Red arrows represent the magnetization directions. The actuation field is applied towards +x axis.

block was prepared by the lost-wax process and the flapping robot was deployed to the hollow structure. Then the whole setup was placed into the coil system and the ultrasonic transducer scanned from the top surface of the agar gel block (indicated as Fig. 2 (e)). The scanned image is shown as Fig. 2 (g) where the robot is detected as the small light area. It is observed that the robot successfully navigates from the left bottom to the right bottom of the channel.

B. Integration of soft and rigid materials

The combination of soft and rigid materials facilitates large deformations or complex motions for the robot design and increases the compliance to the environment with large uncertainty. Here we used two types of UV-crosslinked polymer, a soft type and a rigid type. NdFeB nanoparticles were embedded to generate the magnetism.

1) *Flexural modulus*: Rectangle beams with the dimension of 4 mm×1 mm were fabricated as the bending samples for flexural modulus measurement. We embedded NdFeB nanoparticles in the polymer matrix with a mass fraction of 40% to observe the stiffness of magnetic composite. The embedded magnetic particles were aligned in two manners, which were along the geometric long axis and short axis, respectively. We used three-point flexural tests to measure the flexural modulus for materials with different polymer matrix types and NdFeB mass fractions. The support span is 3 mm and the tip of the microforce sensor (FT-S1000, FemtoTools, Switzerland) contacts the midpoint of the beam (shown as Fig. 3 (a)). The relationship between strain and stress was plotted and the flexural modulus was computed by measuring the slope of the initial straight-line portion of the strain-stress curve. Table 1 shows the computed flexural modulus for different types of materials. It is observed that the change of flexural modulus of the soft type material is within 4% after adding NdFeB particles to the photopolymer. However, there is a marked decrease of flexural modulus of ~68% after embedding NdFeB particles to the hard type polymer matrix. In addition, the geometric alignment of nanoparticles has little impact on the flexural modulus.

2) *Deflection pattern*: Single- and multi-material beams with both in-plane magnetizations were fabricated using

TABLE I: Flexural Modulus of Different Types of Materials

Material	NdFeB Mass Fraction	Flexural Modulus (GPa)
	0	6.912
Rigid Type	40% (long axis)	2.235
	40% (short axis)	2.249
	0	0.303
Soft Type	40% (long axis)	0.305
	40% (short axis)	0.293

DLP, of which the deflection patterns under different actuation fields were presented as Fig. 3 (b). The overall length of the beam is 1.2 mm, and the actuation field is generated by a permanent magnet. The deflection increases as the actuation field changes from 0 to 150 mT. Rather than the smooth curvature of single-material beam, the multi-material beam forms a discrete pattern with a straight shape at rigid segment. Meanwhile, the deflection result shows a larger deformation of multi-material beam than single-material beam under the same actuation field, which indicates enhanced flexibility at the interface between two materials.

IV. DISCUSSION AND CONCLUSION

The fabrication method proposed in this work introduces a digitalized pixel-level strategy to incorporate multiple materials for magnetic soft robot manufacturing, which enables the first steps towards production of more complicated multi-material devices. Improvements of hydrodynamic and mechanical performance are observed by integrating materials with different magnetic and mechanical characteristics. The enhanced flexibility and functionality pave the way for more complex manipulations of printed robots in confined workspace.

However, the current fabrication scheme is still restricted to the manufacturing of 2D-folded shapes instead of multi-layer 3D structures. It is a big challenge building multi-layer structures with multiple materials using digital light processing since it is difficult to selectively pattern various materials on each layer, and repetitive operations such as sample washing and aligning would increase the time cost and reduce the level of automation.

The future work will focus on evaluating the biocompatibility of materials, integrating materials with more varieties of physicochemical characteristics, as well as improving the fabrication efficiency from a general 3D perspective. Meanwhile, in vitro and in vivo experiments will be conducted to study the realistic performance of printed robots and promote application development in targeted or minimal invasive treatments.

REFERENCES

- [1] Q. Ze, X. Kuang, S. Wu, J. Wong, S. M. Montgomery, R. Zhang, J. M. Kovitz, F. Yang, H. J. Qi, and R. Zhao, "Magnetic shape memory polymers with integrated multifunctional shape manipulation," *Advanced Materials*, vol. 32, no. 4, p. 1906657, 2020.
- [2] Q. Ge, A. H. Sakhaei, H. Lee, C. K. Dunn, N. X. Fang, and M. L. Dunn, "Multimaterial 4d printing with tailorable shape memory polymers," *Scientific reports*, vol. 6, no. 1, pp. 1–11, 2016.
- [3] D. Han, C. Farino, C. Yang, T. Scott, D. Browe, W. Choi, J. W. Freeman, and H. Lee, "Soft robotic manipulation and locomotion with a 3d printed electroactive hydrogel," *ACS applied materials & interfaces*, vol. 10, no. 21, pp. 17 512–17 518, 2018.
- [4] S. Wu, C. M. Hamel, Q. Ze, F. Yang, H. J. Qi, and R. Zhao, "Evolutionary algorithm-guided voxel-encoding printing of functional hard-magnetic soft active materials," *Advanced Intelligent Systems*, vol. 2, no. 8, p. 2000060, 2020.
- [5] Y. Yang, D. Li, and Y. Shen, "Inchworm-inspired soft robot with light-actuated locomotion," *IEEE Robotics and Automation Letters*, vol. 4, no. 2, pp. 1647–1652, 2019.
- [6] E. B. Joyee and Y. Pan, "A fully three-dimensional printed inchworm-inspired soft robot with magnetic actuation," *Soft robotics*, vol. 6, no. 3, pp. 333–345, 2019.
- [7] J. Zhang and E. Diller, "Untethered miniature soft robots: Modeling and design of a millimeter-scale swimming magnetic sheet," *Soft robotics*, vol. 5, no. 6, pp. 761–776, 2018.
- [8] X. Wang, X.-H. Qin, C. Hu, A. Terzopoulou, X.-Z. Chen, T.-Y. Huang, K. Maniura-Weber, S. Pané, and B. J. Nelson, "3d printed enzymatically biodegradable soft helical microswimmers," *Advanced Functional Materials*, vol. 28, no. 45, p. 1804107, 2018.
- [9] S. Kim, S. Lee, J. Lee, B. J. Nelson, L. Zhang, and H. Choi, "Fabrication and manipulation of ciliary microrobots with non-reciprocal magnetic actuation," *Scientific reports*, vol. 6, no. 1, pp. 1–9, 2016.
- [10] Z. Ren, W. Hu, X. Dong, and M. Sitti, "Multi-functional soft-bodied jellyfish-like swimming," *Nature communications*, vol. 10, no. 1, pp. 1–12, 2019.
- [11] C. Ma, S. Wu, Q. Ze, X. Kuang, R. Zhang, H. J. Qi, and R. Zhao, "Magnetic multimaterial printing for multimodal shape transformation with tunable properties and shiftable mechanical behaviors," *ACS Applied Materials & Interfaces*, 2020.
- [12] W. Hu, G. Z. Lum, M. Mastrangeli, and M. Sitti, "Small-scale soft-bodied robot with multimodal locomotion," *Nature*, vol. 554, no. 7690, pp. 81–85, 2018.
- [13] E. B. Joyee, A. Szmelter, D. Eddington, and Y. Pan, "3d printed biomimetic soft robot with multimodal locomotion and multifunctionality," *Soft Robotics*, 2020.
- [14] Y. Kim, H. Yuk, R. Zhao, S. A. Chester, and X. Zhao, "Printing ferromagnetic domains for untethered fast-transforming soft materials," *Nature*, vol. 558, no. 7709, pp. 274–279, 2018.
- [15] Z. Ding, C. Yuan, X. Peng, T. Wang, H. J. Qi, and M. L. Dunn, "Direct 4d printing via active composite materials," *Science advances*, vol. 3, no. 4, p. e1602890, 2017.
- [16] C. Christianson, N. N. Goldberg, D. D. Deheyn, S. Cai, and M. T. Tolley, "Translucent soft robots driven by frameless fluid electrode dielectric elastomer actuators," *Science Robotics*, vol. 3, no. 17, 2018.
- [17] Y. Liu, B. Shaw, M. D. Dickey, and J. Genzer, "Sequential self-folding of polymer sheets," *Science Advances*, vol. 3, no. 3, p. e1602417, 2017.
- [18] C. Li, G. C. Lau, H. Yuan, A. Aggarwal, V. L. Dominguez, S. Liu, H. Sai, L. C. Palmer, N. A. Sather, T. J. Pearson, *et al.*, "Fast and programmable locomotion of hydrogel-metal hybrids under light and magnetic fields," *Science Robotics*, vol. 5, no. 49, 2020.
- [19] M. Soreni-Harari, R. St. Pierre, C. McCue, K. Moreno, and S. Bergbreiter, "Multimaterial 3d printing for microrobotic mechanisms," *Soft robotics*, vol. 7, no. 1, pp. 59–67, 2020.
- [20] P. Lloyd, A. K. Hoshier, T. da Veiga, A. Attanasio, N. Marahrens, J. H. Chandler, and P. Valdastrì, "A learnt approach for the design of magnetically actuated shape forming soft tentacle robots," *IEEE Robotics and Automation Letters*, vol. 5, no. 3, pp. 3937–3944, 2020.
- [21] Z. Ji, C. Yan, B. Yu, X. Wang, and F. Zhou, "Multimaterials 3d printing for free assembly manufacturing of magnetic driving soft actuator," *Advanced Materials Interfaces*, vol. 4, no. 22, p. 1700629, 2017.
- [22] J. Zhang, Z. Ren, W. Hu, R. H. Soon, I. C. Yasa, Z. Liu, and M. Sitti, "Voxelated three-dimensional miniature magnetic soft machines via multimaterial heterogeneous assembly," *Science robotics*, vol. 6, no. 53, p. eabf0112, 2021.
- [23] C. C. Alcântara, F. C. Landers, S. Kim, C. De Marco, D. Ahmed, B. J. Nelson, and S. Pané, "Mechanically interlocked 3d multi-material micromachines," *Nature communications*, vol. 11, no. 1, pp. 1–8, 2020.
- [24] Z. Liu, M. Li, X. Dong, Z. Ren, W. Hu, and M. Sitti, "Creating three-dimensional magnetic functional microdevices via molding-integrated direct laser writing," *Nature Communications*, vol. 13, no. 1, pp. 1–11, 2022.
- [25] S. Sundaram, M. Skouras, D. S. Kim, L. van den Heuvel, and W. Matusik, "Topology optimization and 3d printing of multimaterial magnetic actuators and displays," *Science advances*, vol. 5, no. 7, p. eaaw1160, 2019.
- [26] E. B. Joyee and Y. Pan, "Additive manufacturing of multi-material soft robot for on-demand drug delivery applications," *Journal of Manufacturing Processes*, vol. 56, pp. 1178–1184, 2020.
- [27] T. Xu, J. Zhang, M. Salehzadeh, O. Onaizah, and E. Diller, "Millimeter-scale flexible robots with programmable three-dimensional magnetization and motions," *Science Robotics*, vol. 4, no. 29, 2019.
- [28] Y. Chen, H. Wang, E. F. Helbling, N. T. Jafferis, R. Zufferey, A. Ong, K. Ma, N. Gravish, P. Chirarattananon, M. Kovac, *et al.*, "A biologically inspired, flapping-wing, hybrid aerial-aquatic microrobot," *Science Robotics*, vol. 2, no. 11, 2017.
- [29] X. Yan, Q. Zhou, M. Vincent, Y. Deng, J. Yu, J. Xu, T. Xu, T. Tang, L. Bian, Y.-X. J. Wang, *et al.*, "Multifunctional biohybrid magnetite microrobots for imaging-guided therapy," *Science Robotics*, vol. 2, no. 12, 2017.